Reactive Gas Sputtering of Lithium Compound Thin Films

by

Gregory B. Thompson

Brigham Young University

Physics and Astronomy Department

Provo, Utah

June 20, 1996

This research is submitted to Brigham Young University Physics and Astronomy Department is fulfillment of Gregory B. Thompson's senior undergraduate thesis.

Student: Gregory B. Thompson

Signature: Gregory Thompson

Advisor: Dr. David D. Allred

Signature: David D. Allred

Abstract

This research thesis reports the reactive gas sputtering deposition and optical characterization of lithium compound thin films (LiH and LiF). These materials, due to their low absorption, may have a role as spacer layers in soft x-ray multilayer reflectors. Theoretical reflection calculations suggests that a crystalline multilayer stack of a nitride and a lithium compound spacer layer could produce respectable reflectance for short soft x-ray wavelengths (λ<10nm). These types of crystalline frame-works would have an alternating high and low density electron structure with atomically abrupt interfaces, i.e. sharp contrast. If the material is grown epitaxially, layer by layer, a d spacing on the crystalline lattice parameters could be achieved. Unfortunately, the lithium compound films grown in this project showed extremely rough surface morphology. This may have been a result of sputtering conditions (small mean free path), oxide contamination within the sputtering chamber, and/or substrate hinderance. This type of rough growth is not suitable for the developing of uniform planar contrast needed within a multilayer stack. The thin films were chemically and structurally characterized by UV fluorescence, SEM, TEM, and Electron Backscatter Diffraction.

List of Figures

List of Tables

Introduction

With the advent of the visible light microscope (400nm-700nm) by Robert Hooke in the mid 1600s, humankind has been able to investigate objects which were invisible to the naked eye (Grave 1984). It was soon learned that as the wavelength decreases, so does the ability to see smaller and smaller objects. The desire to probe nature at an even smaller scale has made the range of wavelengths of 1 to 100 nm attractive. This range of wavelengths is referred to as soft x-rays. These wavelengths have an energy of 12 to 1200 eV according to

$$E=h\upsilon \qquad (1)$$

where h is Planck's constants and υ is the frequency of the light (Goswami 1992).

The high energy of soft x-rays is sufficiently larger then the bonding energies of outer electrons in atoms and molecules. This allows these wavelengths to have the tendency to penetrate a modest distance into materials. Therefore traditional reflecting lenses and mirrors used in visible microscopy are useless for x-ray microscopy. Since the later part of the 1960s multilayer mirrors have been prepared as imaging devices for soft x-rays (Ceglio 1989).

Background

A multilayer mirror is a periodic, alternating structure of a high density and low density material stacked one on top of another. Each individual layer is a thin film with a thickness

on the order of the x-ray wavelength. The contrast in density between the layers allows a x-ray to be "reflected" according to the Bragg condition

$$m\lambda = 2nd\sin\theta \qquad (2)$$

where m is an integer, λ is the wavelength, n is the index of refraction, d is the bilayer thickness of the two density thin films (commonly called the d spacing), and θ is the incident angle (Fishbane, et. al. 1993). Since n is close to 1, it is often omitted in equation (2). In figure 1, a simplified illustration demonstrates how the x-ray "travels through" a low density material and "bounces off" a high density material. Figure 2 contains Transmission Electron Microscope cross section images of a multilayer stack. By having a x-ray come in at a Bragg angle, θ, for a specific d spacing, a coherent superposition of reflected x-rays can be generated to yield a respectable reflectance.

Bragg's model is a simplified version of the physics which occurs within the multi-reflections of the multilayer stack. Fresnel coefficients of reflection and transmission need to be taken into account for each layer. The true reflectance and transmission of the multilayer stack involves the combining of these coefficients for each thin film through matrix multiplication (Guenther 1990). Since there can be a large number of reflections and transmissions within a multilayer stack, a computer program, LSMM, was used to determine the theoretical reflectance. However, Bragg's condition is a very

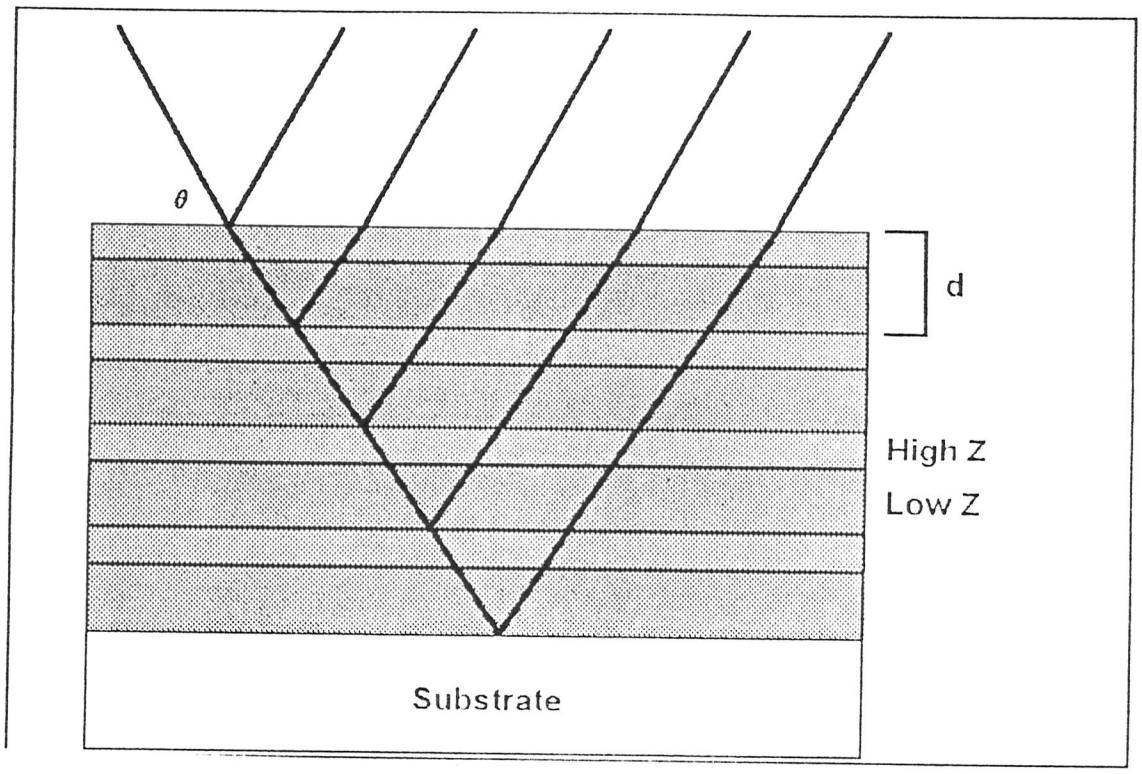

Figure 1. A diagram of how a multilayer "reflects" x-rays according to Bragg's condition (Pew 1994).

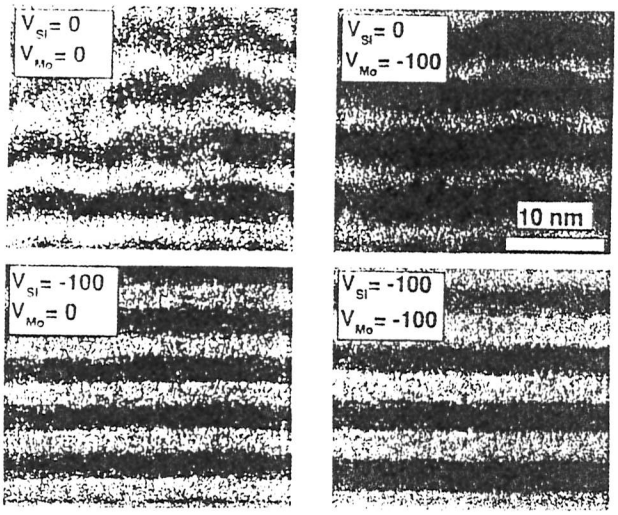

Figure 2. TEM cross sectional images of a Mo/Si multilayer stack (Vernon, et. al. 1993).

good model to determine the angle of reflection and/or the d spacing of the multilayer.

Current multilayer technology has produced reflectance of 60% to 80% for wavelengths of 14 nm. A typical multilayer for these ranges includes the molydenium and silicon (Mo\Si) structure (Conference on the Physics of Multilayers 1996). As the wavelength decreases, the reflectance percentage also decreases. When the decrease is less then 10%, most applications for the multilayer mirror optics become useless (Allred 1996).

An exciting area for soft x-rays in the range of 3 to 4.4 nm is the water window. The water window is a region near the carbon and oxygen Kα lines of 543.1 eV and 284.2 eV respectively. In this intervening energy range, carbon absorbs much more strongly than oxygen. Since most biological cells are primarily composed of carbon in a aqueous environment, a strong optical imaging contrast can exist. Current microscopy methods of Transmission Electron Microscopy (TEM) and Scanning Electron Microscopy (SEM) have difficulty distinguishing between these two elements (Pew 1994). Unfortunately, the multilayers at these wavelengths have been unable to develop respectable images because of poor reflection.

The current research trend in soft x-ray technology has been in developing multilayer mirrors which would produce respectable reflectance for these smaller and smaller wavelengths. Brigham Young University's Physics and Astronomy Department has been investigating the use of rocksalt crystalline structures (B1

compounds), grown epitaxially, for such multilayers. Crystalline epitaxial multilayers have been prepared for over two decades in the semiconductor industry. These structures have generally been ignored for soft x-ray reflectors because of their low theoretical reflectance. Recently, some theoretical calculations using LSMM have shown that some nitride structures paired with an appropriate spacer layer, such as another nitride or hydride, can produce respectable reflectance.

In general, these B1 multilayer structures have properties which could make them ideal for multilayer optics. The periodicity of high and low electron density material allows for strong, sharp contrast to exist between layer pairs, i.e. atomically abrupt interfaces. Epitaxial crystalline multilayers with sharp contrast between layer pairs have been prepared for studies in superconducting Josephson junctions and advanced hardness coatings (Kawaguchi and Shin 1990; Talvacchio and Braginski 1987; Kim, et. al. 1988). Ideally, if the material is grown epitaxially, layer by layer, a d spacing on the order of the crystalline lattice dimensions could be achieved, i.e. a few angstroms. Traditional multilayer thought has been that the films, especially the spacer layer, need to be amorphous to allow smooth and uniform growth (Allred 1996).

Principles of Multilayer Construction

As mentioned above, high contrast between the layers in a soft x-ray multilayer should exist. The larger the contrast, the

greater the reflectance for a given number of layer periods. Figure 3 is a plot of the elements with their respected index of refraction, n, at 10Å. The index of refraction is an inherent property of a material to change the wavelength of the incident light when traveling through the material's inner structure (Guenther 1990). The index of refraction consists of a real and an imaginary component,

$$n^* = n + i\beta \qquad (3)$$

Since the index of refraction of most materials in the x-ray range is almost but slightly less then unity, n is written as

$$n = 1 - \delta \qquad (4)$$

The imaginary term, β, is associated with absorption. When researching new materials for optical multilayer mirrors, plots like figure 3 become indispensable. They provide a visual image of how elements compare to each other at a certain wavelength.

An example of high contrast can be seen with uranium, U, and scandium, Sc. These elements are near the extreme ends on the plot found in figure 3. These two materials could produce a good multilayer from an optical point of view because of their high contrast. Even though two materials may look good on an optical plot, they may not actually form a good multilayer. One of the first multilayers made for x-ray mirrors was Cu/Ag. These two materials, over time, diffused into each other. This effect destroys the contrast value which is essential to multilayer reflection. Besides the bulk diffusivity of materials and

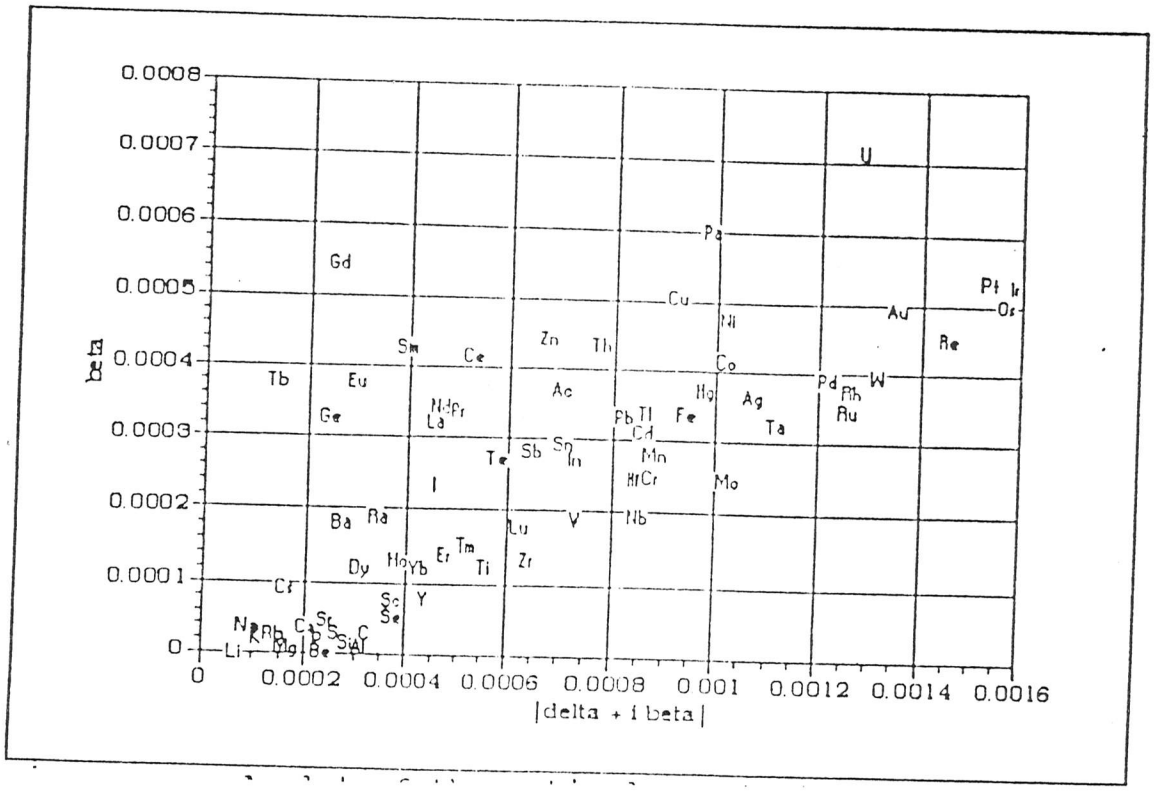

Figure 3. Optical constants of the elements at 10Å (Pew 1994).

optical contrast, surface mobility, nucleation of the material to a substrate, and the feasibility of depositing the material as a uniform thin film need to be considered (Ohring 1992). These latter considerations were extremely important to this research project.

Nucleation

Nucleation is the subject that deals with the mechanics by which atoms that are deposited on a surface cluster and bond to each other and the substrate surface (Ohring 1992). The major idea of this subject revolves around Gibbs free energy. As atoms cluster together, energy is required for this movement. Once a critical radius of a cluster is achieved, this energy requirement decreases and it becomes energticly favorable for the atoms to "join" into larger and larger cluster sites. A continuum model which describes this mathematically yields the equation

$$\Delta G_V = -(k_B T/\Omega)\ln(1+S) \qquad (5)$$

for homogenous nucleation. (This simplified model does not take into account complex heterogeneous sites such as those that exist on substrate surfaces.) ΔG_V is the change in chemical free energy per unit volume, k_B is Boltzmann's constant, T is temperature, Ω is the atomic volume, and S is given by $(P_V-P_S)/P_S$ or the vapor supersaturation. P_S is the vapor pressure of the solid and P_V is the pressure of the supersaturated vapor. If S is zero (nonexistent), nucleation is impossible. If $P_V>P_S$, then ΔG_V is negative, i.e. there is an energy reduction for

condensation. This can give raise to large surface formation, i.e. nucleation. These new sites increase the surface free energy of the system. It is given by

$$4\pi r^2 \gamma \qquad (6)$$

where γ is the surface energy per unit area. The total free energy of the system is

$$(4/3)\pi r^3 \Delta G_v + 4\pi r^2 \gamma \qquad (7)$$

where $(4/3)\pi r^3 \Delta G_v$ is the chemical free energy from a gas to a solid transformation. To find the minimum of ΔG needed for nucleation, we have

$$d(\Delta G)/dr = 0 \qquad (8)$$

This yields

$$r^* = -2\gamma/\Delta G_v \qquad (9)$$

where $r=r^*$ for this derivative case. Equation 9 is substituted back into equation 7 and the result is

$$\Delta G^* = 16\pi\gamma^3/3(\Delta G_v)^2 \qquad (10)$$

The quantity ΔG^* represents the minimum energy barrier needed to be overcome before clustering becomes energically favorable. The quantity r^* is the cluster nucleus size needed to exist before nucleation is energically favorable. Figure 4 illustrates graphically the nucleation method in terms of the mathematically model discussed.

Heterogenous nucleation is more complicated by the fact deposition and substrate surfaces are considered. Substrates will give rise to nucleation sites on kinks, ledges,

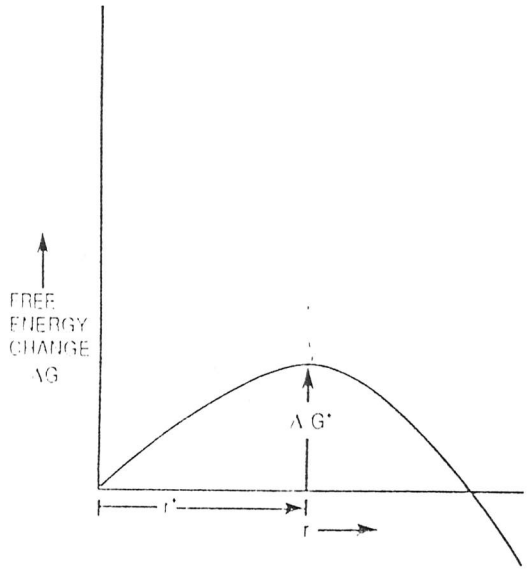

Figure 4. An graphical illustration of nucleation. This picture illustrates the free-energy change (ΔG) as a function of cluster ($r^* > r$) or stable nucleus ($r > r^*$) size. r^* is the critical nucleus size, and ΔG^* is the critical free-energy barrier for nucleation (Ohring 1992).

dislocations, etc. which can drastically change the energy considerations for the formation of stable nuclei. Capillarity theory is used to model this type of nucleation. The reader is advised to consult *The Material Science of Thin Films* by Ohring for more details in the theory of nucleation. This book will also give the background associated with diffusion of films, surface mobility, and other relevant thin film formation and structural information.

Magnetron Sputtering Deposition

Sputtering is one of the most common methods for the deposition of thin films. Sputtering occurs when atoms are ejected from a material surface by collisions of positive ions which are accelerated into the surface by a potential difference. This material surface is known as a target. The collision of an ion with the target's surface causes a cascade of secondary collisions between target atoms by the ion's transfer of momentum. These secondary collisions continue until a target atom is ejected from the surface. The ejected atom travels through space until it condenses onto a substrate by nucleation, i.e. thin film growth. The main advantages of sputtering include (a) high thickness uniformity, (b) good adhesion to a substrate, (c) reproducibility of films, (d) ability to deposit and maintain the stoichiometry of the original target, and (e) relative simplicity of film thickness control (George 1992).

Diode sputtering is one of the common methods of sputtering to obtain thin film deposition. The diode sputtering technique involves the breakdown of a high atomic number gas (positive ions), usually argon, into a partially ionized plasma. This is achieved by a voltage separation of 300V to 800V between the negatively charged target (cathode) and a grounded shield. The argon pressure is usually held between 1 to 20 mTorr (George 1992). Before sputtering, the chamber is placed under a vacuum. This allows the argon pressure to be under a controlled flow into the chamber. The vacuum environment also reduces the contaminates the film will experience during deposition, increases the mean free path of the sputtered atoms, and the break down of the gas into a plasma by relatively small voltages.

In magnetron sputtering, a type of diode sputtering, the plasma is harnessed into a toroid shape above the target by the arrangement of permenitate magnets beneath the target, hence magnetron sputtering (Ohring 1992). Magnetron sputtering was first introduced in 1974 by Penning, but the basic principles were demonstrated by Kesser and Pashkova in 1959 (George 1992). The magnets use the electrical properties of the partially ionized plasma to achieve the desired sputtering effect. The magnetic field lines form a closed path on the cathode surface. The differences in mobilities, by the Lorentz force, of the "light" electrons and the "massive" positive ions causes a positive ion sheath to develop close to the target cathode. This produces a floating negative potential relative to the plasma.

All these effects together cause positive ions to be extracted from the plasma and accelerated to the target (George 1992).

The accelerated ions strike the target (cathode) ejecting the target atoms. The magnetron effect of crossed electric and magnetic fields prevents the electrons from reaching the anode by the closed path on the cathode. The magnetic field of the magnets first runs normal to the target, then bends parallel to the target (the magnetron component), and then back normal to the target. The magnetron component prevents the electrons from escaping and accelerating to the anode. The electrons are then trapped in cycloidal motion orbits in the dark space (area where electric and magnetic fields both exist) (Ohring 1992).

In the zones of efficient electron trapping, the electron density reaches a critical value, at which the ionization of trapped electrons is at a maximum. This allows a higher rate of secondary electron production to occur within the plasma without the need for high energy positive ions (Ohring 1992). The generation of secondary electrons makes the plasma self stabilizing. When this is reached, effective sputtering can be accomplished. Magnetron sputtering was the employed technique used to produce the project's thin films and multilayer stacks.

The major disadvantage of magnetron sputtering is the requirement that the target to be sputtered be conductive. Insulators do not allow a potential difference to exist for the acceleration of the ion into the material.

Experimental Magnetron Sputtering System

The magnetron sputtering system used in this project was a stainless steel chamber that housed two metallic targets. The targets had a grounded tubular casement over them to allow a columnated sputtering trajectory. These tubes had a step ledge which protruded roughly half an inch over and a half an inch above the target to produce the potential difference and define the plasma area. The chamber used a mechanical roughing pump and a cryopump to evacuate the system. The base vacuum pressure of the chamber is ~$5x10^{-7}$ Torr. The major contaminate of the system at these pressures was water. Heat tape was used to warm the chamber's walls to help bake out the system. The substrates are rotated with planetary motion above each of the targets by a computer controlled stepping motor. The substrates are ~25cm from the target surface. A Ferrin Scientific Mass Polarity Analyzer (MPA) is attached to the chamber. This device can analyze the individual gases present in the system by their respected masses. Sputtering gases are flowed into the chamber via mass flow controllers and/or needle valves.

Besides the argon gas in the system (plasma source), the project required the use of a secondary or reactive gas at a slightly lower pressure. This is known as reactive sputtering. The added gases are used to allow the sputtered, elemental atoms to form compounds with the reactive gas. Reactive sputtering gases can be used to make oxides, nitrides, carbides, etc. (George 1992). Reactive gas magnetron sputtering has produced

multilayers of a d spacing of 9.6Å (Hirashita and Greene 1991). This makes magnetron sputtering an ideal technique to begin research on small d spacing crystalline compounds.

Lithium Compound Spacer Layers

As stated in the Background section, the concept of preparing crystalline based multilayer reflectors is being investigated. In order for these structures to produce respectable reflectance, ideal spacer layers (low density material in a multilayer) need to be developed. In figure 3, lithium, Li, is the first solid element in the periodic table with the smallest delta. It is nearly transparent to the penetrating x-ray, i.e. it does not absorb much of the x-ray energy. This makes lithium's optical properties ideal for a spacer layer. It would allow nearly all the x-ray energy to travel through its structure. The majority of the reflections would occur in the high density layers. Unfortunately, lithium is a very reactive element in air. It wants to be "stable" by "giving up" its one electron in its 2s subshell to another element. If lithium is to be harnessed as a component in a multilayer structure, it can not be reactive with the elements. This might be achieved by having it in the form of a stable compound in the multilayer structure. The compounds studied in this project were lithium hydride, LiH, and lithium fluoride, LiF. These compounds have the rocksalt structure (Face Center Cubic, FCC) placing them into the B1 category (Weast 1978). This

makes them ideal candidates for the crystalline based multilayers.

Epitaxy

In order for these crystalline structures to be used as multilayer mirrors, the individual thin films need to grow epitaxially, one layer on top of another. This type of epitaxial growth is essential to insure uniformity and contrast between layer pairs. Epitaxy refers to the extended single-crystal film formation on top of a crystalline substrate. Homoepitaxy is the deposition of a film on a substrate of the same material: heteroepitaxy is the deposition of a film on a substrate of a different material (Ohring 1992). When dealing with heteroepitaxy, lattice misfit between the film(s) and substrate become important. To achieve this type of crystalline growth, epitaxial theory predicts that the lattice mismatch needs to be less then 9% (Ohring 1992; Takayanagi, et. al. 1977; Green, et. al. 1969). Depending on whither the film was smaller or larger then the substrate's parameters, strain or stress will result.

To illustrate an example where lithium compound crystalline structures could be advantageous in short x-ray wavelength regions, consider a LiH and MoN multilayer grown epitaxially on a MgO substrate. (Note that the lattice parameters of LiH, MoN, and MgO are 4.09Å, 4.24Å, and 4.20Å respectively. The lattice mismatch of these FCC compounds is well within 9% needed for

heteroepitaxy.) For a wavelength of 20Å with a d spacing of 10Å for 500 layer pairs, a theoretical reflectance of 26% at near normal incidence could be achieved.

Lithium Target Preparation

As mentioned above, lithium is a very reactive element in atmospheric conditions. This posed the first serious barrier to the project. The target needed to stay in its metallic form, i.e. not an insulator, in order to be magnetron sputtered. The targets were cut from a lithium ingot and pressed in an aluminum container with 2000 psi. The aluminum container was used to fix the lithium metal into the geometrical shape of the target. Cutting and pressing the lithium was fairly easy due to the soft nature of the metal. The only concern was the gumming up of the lithium metal during the cutting process. Either a sharp knife of a band saw was used to cut the lithium from its ingot form. The cutting and pressing of the lithium was done in a readily process to keep the metal from oxidizing in the air. Once the lithium was pressed, the target was placed into the magnetron sputtering chamber. A razor blade then was used to scrape off any oxide build up on the lithium surface. This was evident by a rough, whitish crust on the surface. A dark grey color was present on the surface as well. This too was scraped off to reveal the metallic color of the metal. An ohm meter was used to ensure if the lithium target was conductive.

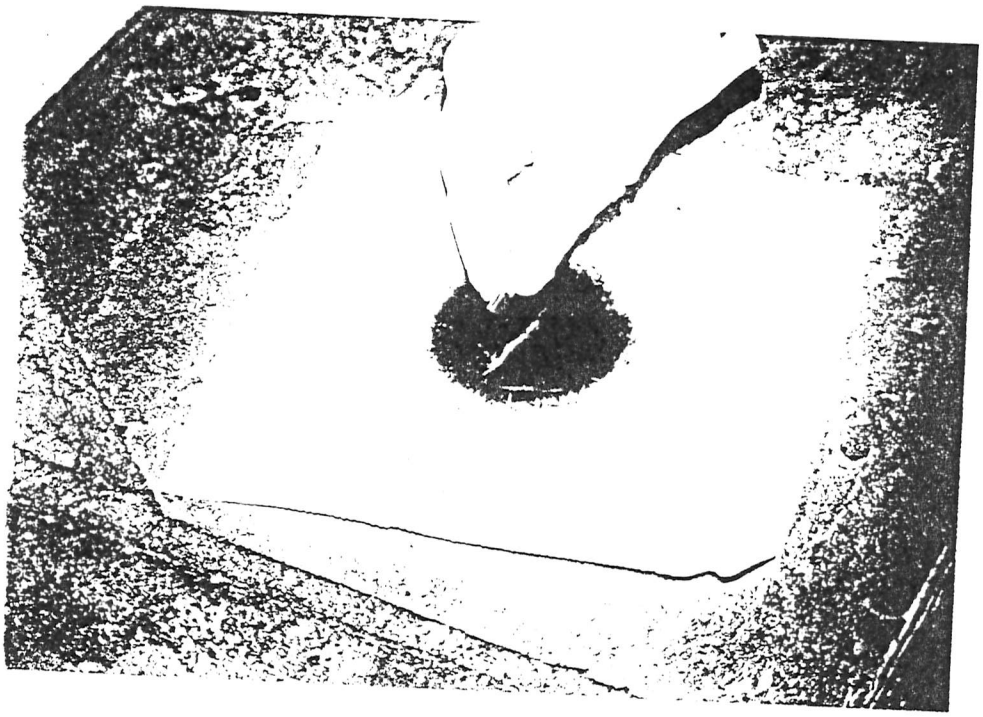

Figure 5. A photograph of a lithium target.

Once the chamber was under a sufficient vacuum, the target was sputtered to remove any residue oxide formations. Indications of a "clean" lithium surface was stable sputtering voltages. If the target had a sufficient oxide build up among its pure elemental components, the sputtering voltages would fluctuate. Typical sputtering voltages and current were 250V to 310V at 0.24A to 0.32A for 80W.

Lithium targets that were not in use where stored by submerging the metal in a glass container of spectrograde hexane. This kept the metal from oxidizing with the air. The metal would produce a thin, dark colored, outer layer when in the hexane bath. This coating did not seem detrimental to the metal and was easily rubbed off when the sample was taken out for use. Figure 5 shows a photograph of a lithium target.

Experimental Set-up

In order to make lithium stable in a multilayer stack, it needed to be harnessed as a compound. This was accomplished through reactive sputtering. For the LiH compound, NH_3 and H_2 gases were used. The LiF compound used NF_3 gas as its source. Each reactive gas would break down in the plasma into its respected atomic components. This would allow each elemental gas component to bond with the sputtered lithium atoms. Ammonia, NH_3, was used to explore the possibility of using one reactive gas to produce a bi-compound multilayer, such as the one mentioned in the reflectance example, i.e. LiH/MoN. The ammonia

could supply the nitrogen component to the Mo sputtered atoms and the hydrogen component to the Li sputtered atoms. To insure that the Li and Mo would bond with their respected gaseous components, a Gibbs free energy chart for these elements in the presence of NH_3 was plotted. As you can see from figure 6 and figure 7, a lithium hydride and a molydenium nitride are the most stable compounds to form as long as the temperatures are kept under 200°C and 250°C respectively. Note that the multilayer required a MoN structure instead of a Mo_2N structure. MoN is a metastable state in which the Gibbs free energy program used did not have access too in its data base. Considering that lower energy states can exist in epitaxial growth because of preferred orientations, the lattice parameters and structure of MoN would be more favorable towards growth than Mo_2N. Figure 8 is a plot of Li in the presence of NF_3. The compound of LiF is the most thermodynamically favorable.

Each of the reactive gases chosen could also pose problems to the sputtering system. For example, consider the pure hydrogen (H_2) source. Since the chamber reaches high vacuum pressures via a cryopump, the mechanics of this pump makes the pumping of pure hydrogen extremely difficult (Chambers 1989). Hydrogen has a low condensation temperature which does not enable the pump to easily evacuate the gas during vacuum pumping. This problem was overcome by slowing flowing the H_2 gas into the system while the Li target was sputtering. The gas was continually added to the chamber till it appeared that the gas

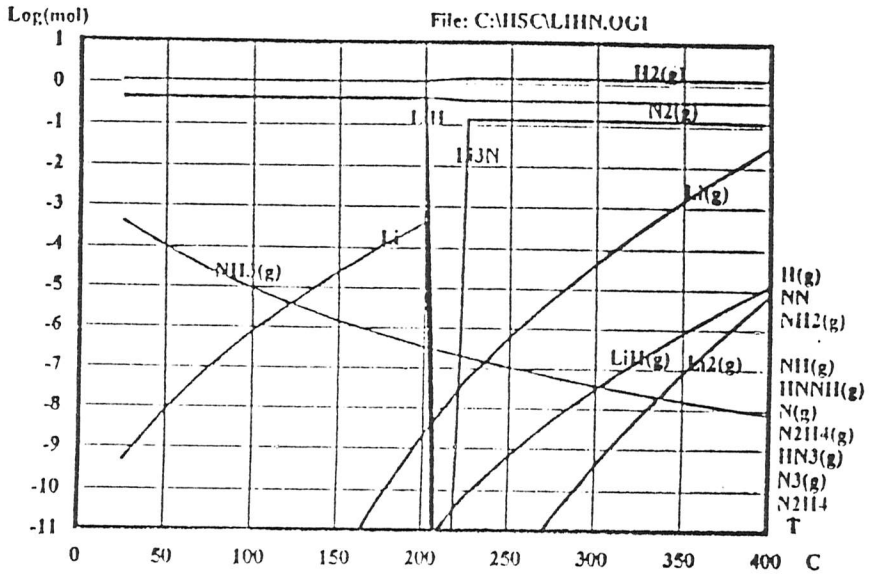

Figure 6. Gibbs free energy plot of Li with NH_3.

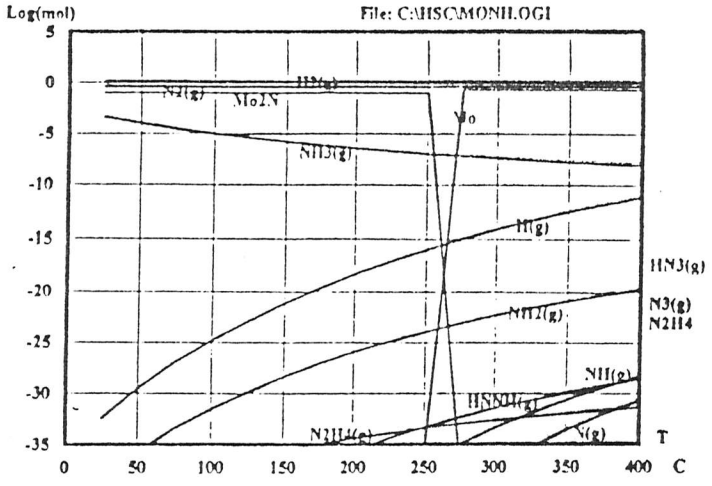

Figure 7. Gibbs free energy plot of Mo with NH_3.

was in excess to what was needed to bond with the sputtered Li atoms. This was indicated by a jump in hydrogen from a base level on the MPA read-out and/or an increase in the cryopump's temperature. The detrimental nature of the two other gases (ammonia, NH_3, and nitrogen triflouride, NF_3) may exhibit corrosive nature to the chamber walls and sputtering instrumentation.

The Li films were deposited on either a Si wafer (100) or a MgO (100) substrate. Silicon wafers' smooth topology lends its self well as substrates for x-ray mirrors. Though silicon does not have the appropriate lattice parameter (5.42Å) for epitixial growth for the lithium compound thin films. These substrates were used to see if deposition of the compounds was possible. The substrates were kept at room temperature (~25°C) during deposition. This means that they were placed in the chamber and not intentionally heated or cooled during sputtering.

Experimental Procedure

A typical sputtering run involved pumping the chamber to $5x10^{-7}$-$1x10^{-6}$ Torr range accompanied by an one hour bake out. The argon gas was flowed into the system up to 1-$2.5x10^{-3}$ Torr. The respected reactive gas' pressures were flowed up to the mid to high 10^{-4} Torr pressure range. Typical sputtering rates of lithium in the presence of the hydrogen and ammonia sources was 25Å/min at 80W. When nitrogen triflouride was used, the sputtering rates decreased to 12Å/min at 80W. Figure 9 shows a

gas trend plot during a sputtering run with ammonia. This plot illustrates two major points. The first is the break down of the ammonia gas. At approximately 125 minutes, the sputtering voltages were turned off which resulted in the lack of a plasma. The nitrogen line drops by an order of magnitude and the ammonia line increased by half an order of magnitude. This demonstrates that the gases were indeed breaking down into their respected components while the plasma was on. The other significant indication on the plot is the presence of a background level of oxygen. The presence of this element could contaminate the Li to form Li_2O instead of a LiH or LiF compound. In many of the sputtering runs, oxygen could not be detected (it was below scale, i.e. below 10^{-7} Torr).

Typical LiH thin films were deposited to a thickness of 1000Å, where LiF thin films where deposited to thickness of 500Å. Thickness measurements were done by a Wykco visible light interfermonmeter. A step ledge between the substrate and the film produced the desired visible light interference.

The lower thicknesses of the LiF films were a result of deposition problems. The corrosive nature of this gas caused the contamination of the sputtering target. If too much reactive gas was added to the sputtering target, the target's voltage will increase and the current will decrease resulting in a poor sputtering yield. These electrical changes indicate that the target is losing its conductive nature and becoming more insulating. As this continues, the plasma becomes intermit and

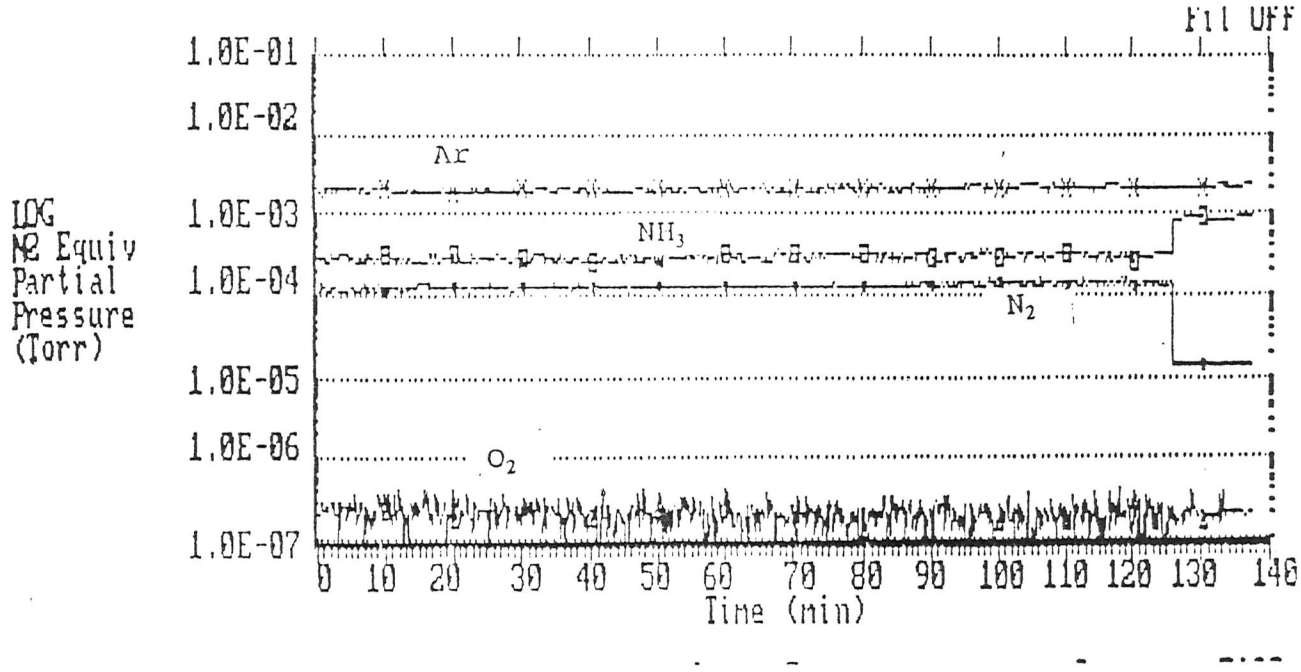

Figure 9. Trend plot of Li being sputtered in NH_3. Note that at ~125 minutes, the sputtering voltages were turned off and the ammonia does not break down (NH_3 pressure increases and N_2 decreases).

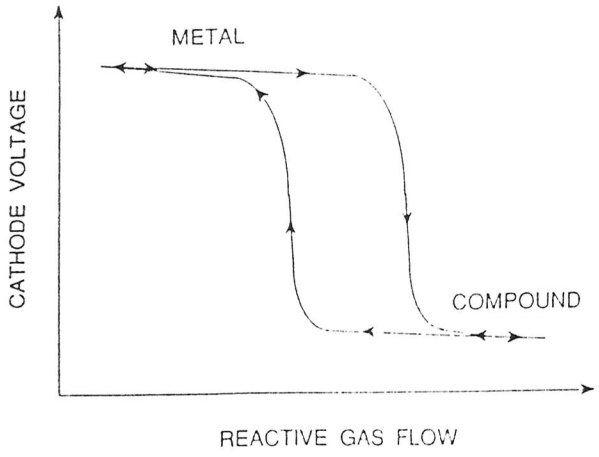

Figure 10. A hysteresis curve of cathode voltage vs. reactive gas flow rate at constant discharge current (Ohring 1992).

the target no longer sputters. Accurately monitoring the NF_3 gas pressure in the chamber was hindered in two ways. The first was NF_3's corrosive nature. It eventually destroyed a monitoring filament in the mass polarizer analyzer, preventing accurate readings of all individual gas pressures. The other hinderance was the input valves. The mass flow controller did not have a positive shut off. This allowed some of the gas to enter the chamber even when the controller valve was shut. A needle valve remedy was used, but the gas corroded the valve over time causing similar gas flow problems. The contamination of the target could be seen in each sputtering deposition run. After contamination the lithium target appeared to have a grey surface coat instead of the metallic shine associated with previous sputtering runs. Figure 10 is a graphic illustration of how electrical components of magnetron sputtering change when too much reactive gas is flowed into the system.

Band Gap Characterization

Once the LiH and LiF thin films were deposited, they needed to be characterized. A chemical analysis of the material, via some type of x-ray technique, could not be done because of the low absorption these materials have to x-rays. The preferred method to "finger print" the LiH film was done by determining the band gap. An IR-Visible-UV spectrometer was used to obtain the reflectance of the LiH film. Figure 11 is a plot from a spectrometer run. Below ~250nm there is a drop in the

reflectance of the LiH film on silicon. This corresponds to a band gap of ~5 eV. The band gap of LiH is 5.05 eV (Pilipenko, et. al. 1985; Polienko, et. al. 1993).

UV fluorescence was used to determine the presence of defects in the material. Figure 12 shows an emission mode plot with excitation at 250nm (~5 eV) for a LiH film deposited on Si. Peaks at 2.5eV, 3.5eV, and 4.4eV were seen. These corresponded quite well with published literature for LiH (Ikeya and Miki 1976). With these results, it was concluded that LiH was produced by reactive sputtering. Figure 12 also showed other peaks for this sample. Upon further investigation, the defect peak at 3.1 eV corresponded to Li_2O, a possible sign of contamination (Ortman and Larsen 1983). Ortman and Larsen have also reported Li_2O absorption spectra results for bands at ~2.2 eV and ~3.9 eV. The relative intensity of the 3.1 eV peak in figure 12 indicates that the contamination was small, but significant. The peak at 1.9 eV has not yet been identified. The contamination from the oxygen could have been a result from residue oxide release from the target's surface during sputtering, water's molecular break down in the system, and/or a minute air leak which was below scale on our MPA. LiF high band gap (14.1eV) prevented the use of these techniques in determining its chemical composition (Himpsel 1993).

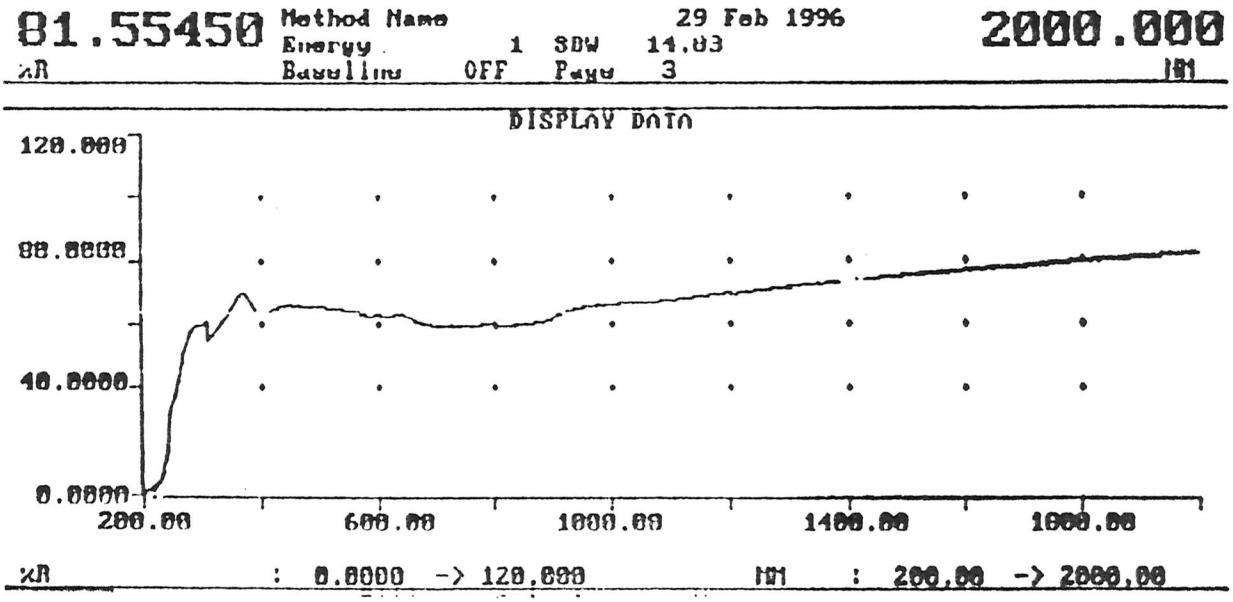

Figure 11. A UV-Visible-near IR Spectrometer plot of 1000Å LiH on a Si substrate. Note the drop in reflectance at ~250nm. This corresponds to a ~5 eV band. Reactive gas was NH_3 at 0.75mTorr.

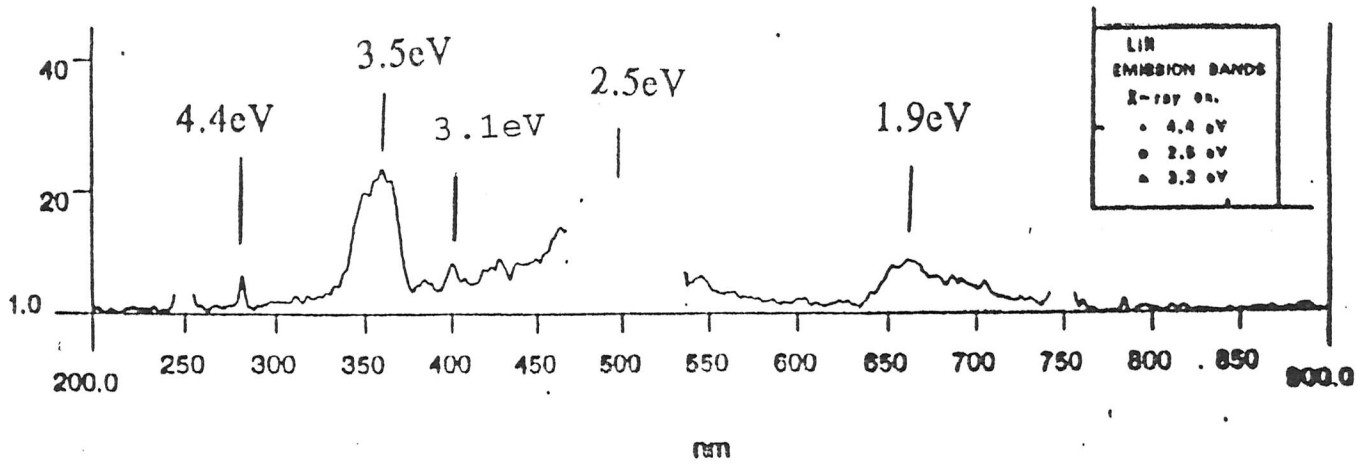

Figure 12. A fluorescence emission plot with excitation at 250nm. A 1000Å LiH film on a Si substrate. Reactive gas was NH_3 at 0.85 mTorr.

Electron Backscatter Diffraction

Further characterization of the LiH and LiF films included Electron Backscatter Diffraction Pattern (Kikuchi Method). This method involves the diffraction of electrons off the material's surface (Field 1995). Depending on the crystal structure, different diffraction patterns would be seen. Figure 13 shows the diffraction pattern of a Si wafer substrate. This pattern is associated with the diamond cubic structure. By using this technique, a diffraction pattern of a FCC structure would further indicate the LiH and/or LiF presence.

Unfortunately, no diffraction pattern was seen for a 1000Å LiH film on Si or MgO substrates. No pattern usually indicates amorphous structure or small grain structure (Kikuchi method has a resolution of ~500Å). Since the film was shown to be LiH by the UV fluorescence method, a crystalline structure should be present. The lack of the diffraction pattern could be the transparency of the film.

Originally a diffraction pattern was thought to have been seen with a 500Å LiF film. Figure 14 is a photo of its suspected diffraction pattern. As the electron beam was moved to other locations, the same pattern and orientation kept on appearing. This could indicate single crystal epitaxial growth. Since the LiF was deposited on a Si wafer, this could not be the case. (The lattice mismatch is greater then 9%.) It was concluded that the faint pattern was the Si wafer structure showing through. The diamond cubic structure's diffraction pattern is very similar

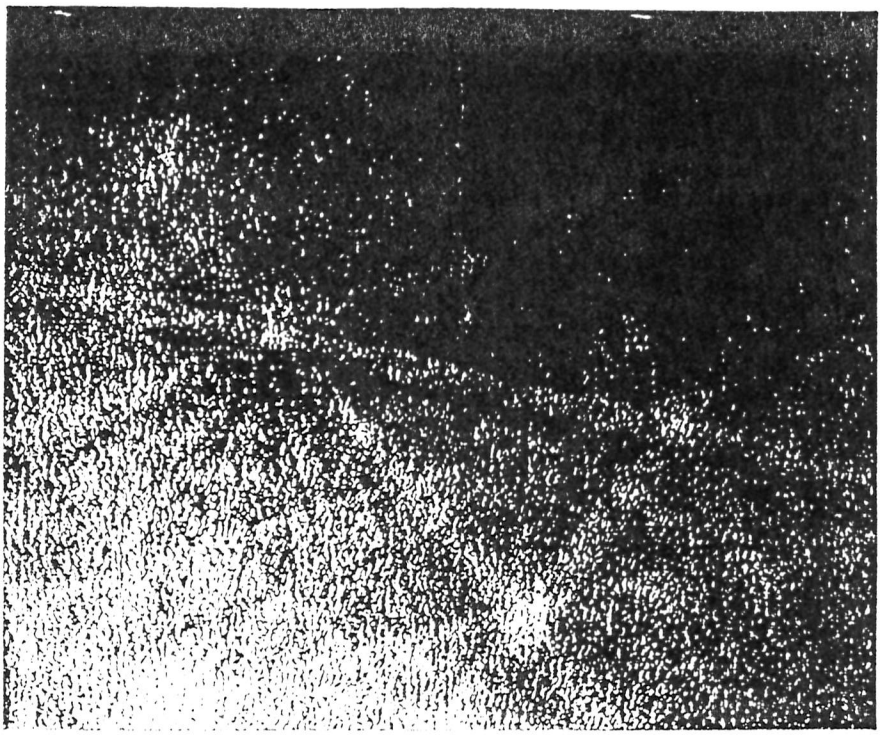

Figure 13. An electron backscatter diffraction pattern of a Si wafer.

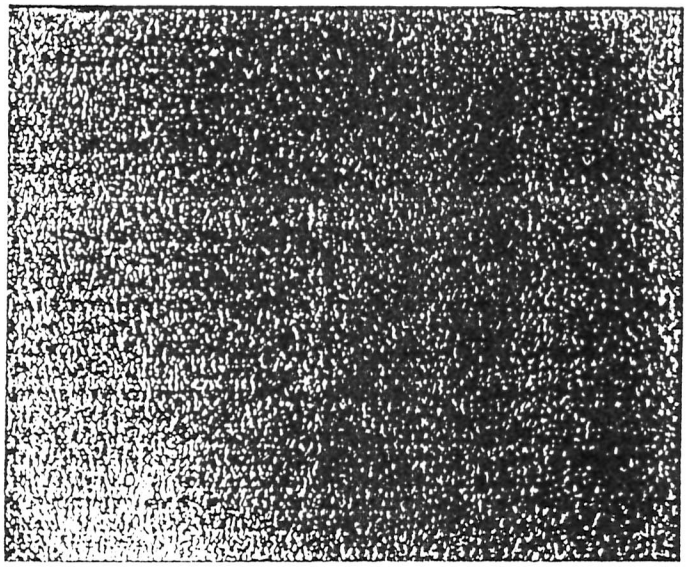

Figure 14. An electron backscatter diffraction pattern of a ~500Å LiF film on a Si substrate. This pattern is the Si structure showing through the LiF film.

to the face centered cubic structure except that it has two faint bands coming out of its center. The signal of these bands were not strong enough to be seen clearly beneath the LiF film. The ability to detect the Si structure pattern through the 500Å LiF film demonstrates the great transparency properties these films could have in x-ray multilayer optics.

Transmission Electron Microscopy Characterization

An earlier method of characterization for the LiH films was done by Transmission Electron Microscopy (TEM). TEM could indicate the crystallinity, i.e. FCC, and lattice parameters of the LiH crystals deposited. A 200Å thick film was deposited onto a copper grid. This film was sputtered by a triode method instead of a magnetron method. The triode method is similar to the magnetron method expect a collimated positive ion plasma beam is accelerated towards a target by a -1.5kV potential. The plasma is collimated by an external magnetic field coil. The plasma beam "hits and knocks out" the target atoms as its sputtering method.

The TEM characterization of the LiH film also proved to be difficult. As the electron beam scanned through the samples, the crystallites appeared to be moving. This could be a result of heating up and decomposition and/or charging up of the sample. Even though a low electron beam energy setting was used and the samples were mounted on a liquid nitrogen stand, this movement of the LiH crystallites still occurred. Figure 15 is a photograph

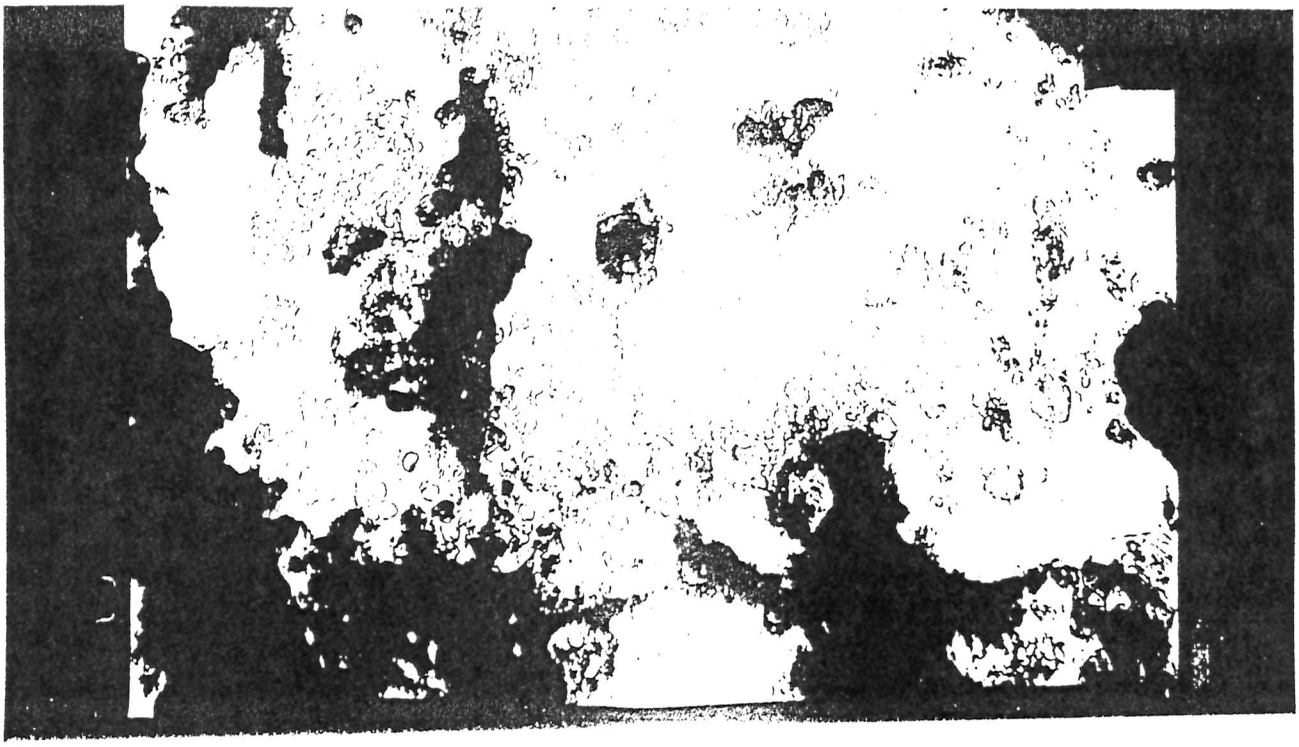

Figure 15. A TEM image of ~200Å film of LiH crystallites. Reactive gas was H_2 at ~0.5 mTorr.

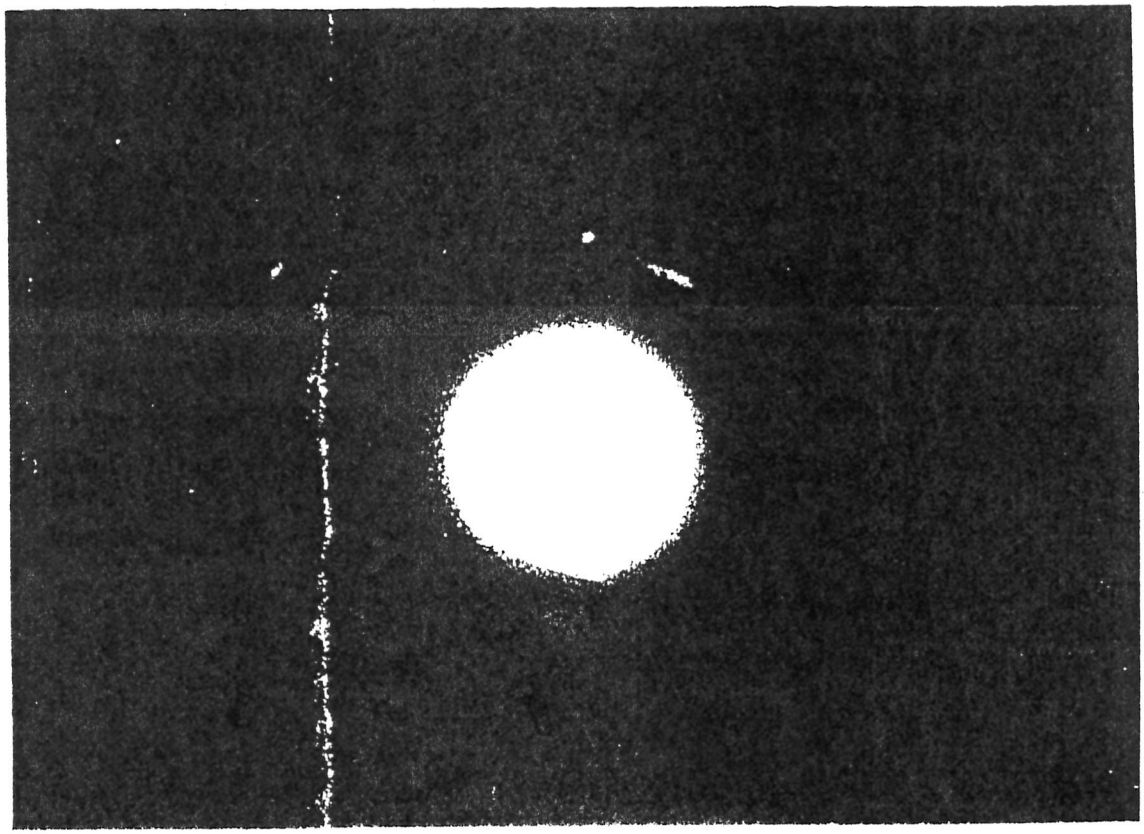

Figure 16. A TEM diffraction image of a ~200Å film of LiH. Reactive gas was H_2 at ~0.5 mTorr.

of these possible LiH crystallites. Figure 16 is a diffraction pattern taken from the TEM characterization work. This photo shows a faint diffraction pattern of concentric circles and characteristic spots, of which nothing conclusive can be determined by the pattern.

Scanning Electron Microscopy Characterization

The final method of characterization of the LiH and LiF films was the study of its surface morphology by Scanning Electron Microscopy (SEM). The films were coated with 30-100Å gold coatings by a sputtering method. This was done to see an image. The transparency nature of the LiH and LiF films would prevent the imaging of its surface without this gold coat. This work proved to be the most interesting characterization of the films.

Figure 17 is a SEM image of a 1000Å LiH film deposited on a Si wafer. The reactive gas was NH_3 at 0.85 mTorr. The image clearly shows that the film grew rough. This would pose a serious hinderance to the development of a periodic multilayer. There would be no clear distinctions between layers if the surfaces were not uniform planar. Figure 18 shows a side profile of the same film. This again demonstrates the rough topology of the LiH film. Other LiH films deposited onto Si wafers at various reactive gas pressures and gases (NH_3 or H_2) showed similar surface morphology. The roughness of the film's surface may be caused by mean free path lengths of the sputtered atoms

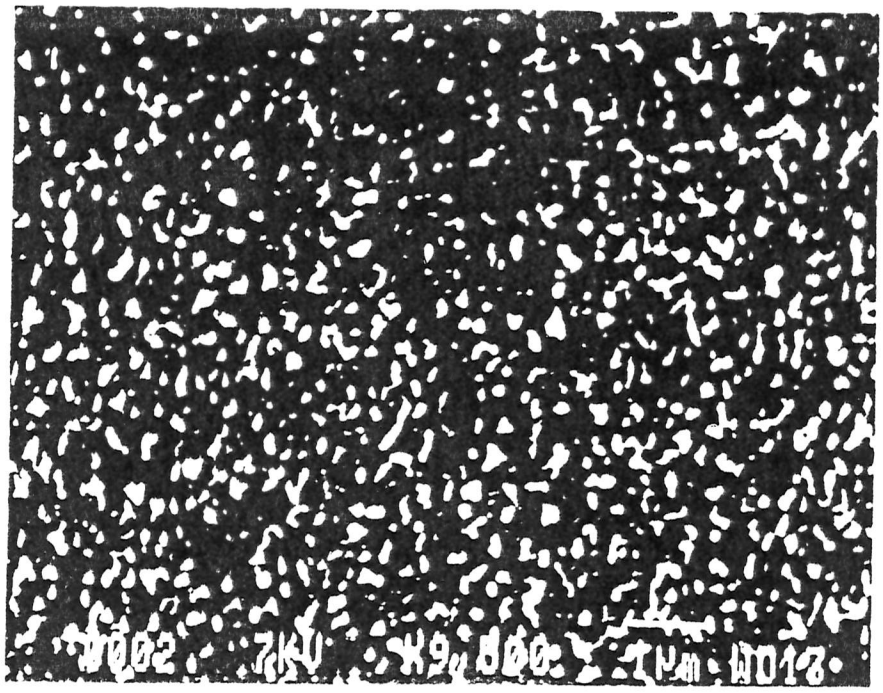

Figure 17. SEM image of a ~1000Å film of LiH. Reactive gas was NH_3 at 0.85 mTorr.

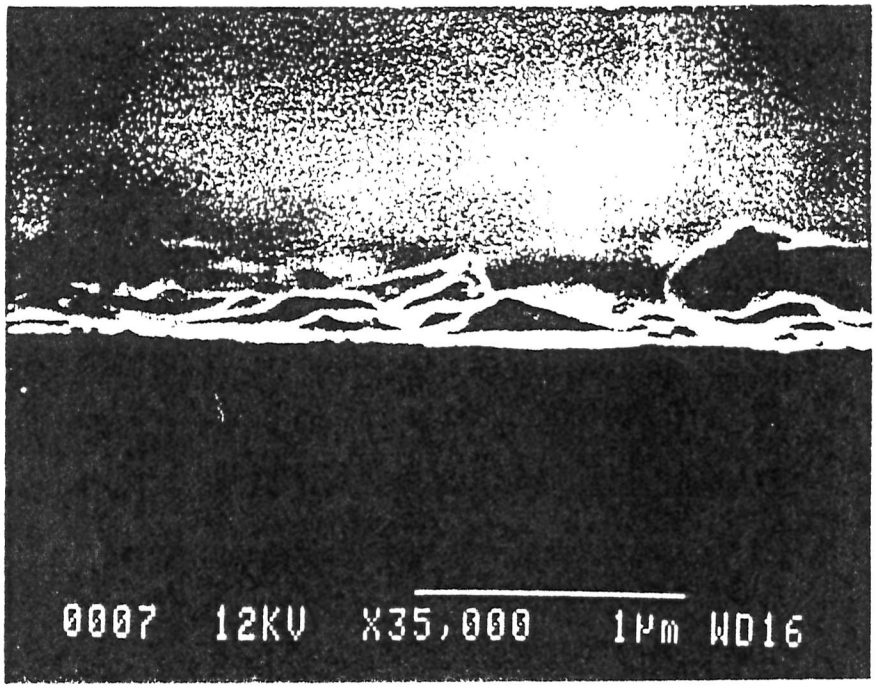

Figure 18. Side profile of the SEM image seen in figure 17.

(distance between atoms), oxide contamination, and/or substrate hinderance.

Discussion of Rough Growth

Movchan and Demchishin described the surface morphology of thick evaporated metal films using the ratio of the substrate temperature to the melting temperature of the metal (Movchan and Demchishin 1969). This description of morphology was broadened by Thorton to discuss the morphology of sputtered thin films. Thorton added the contributing factor of gas pressure. With the ratio of temperatures and gas pressures as parameters, Thorton divided surface morphologies into four zones (Thorton 1977). This is referred to as the zonal model of surface morphology evolution. The morphology of the zones is thought to arise from four basic processes: shadowing, surface diffusion, bulk diffusion, and sublimation activation energies (Ohring 1992).

Shadowing is a phenomenon which results from geometric consideration of the substrate's location to the arriving atoms. The substrates in the project were ~25 cm directly above the target surface area. They would be perpendicular to a sputtered atom whose trajectory was vertical from the target. The geometry of the sputtering components should not cause a strong shadowing effect, i.e. there is no physical obstructions between the target and substrate. The diffusion and sublimation energies are associated with the properties of the material. Figure 19 is a diagram of a zone structure with Table 1 being the zones'

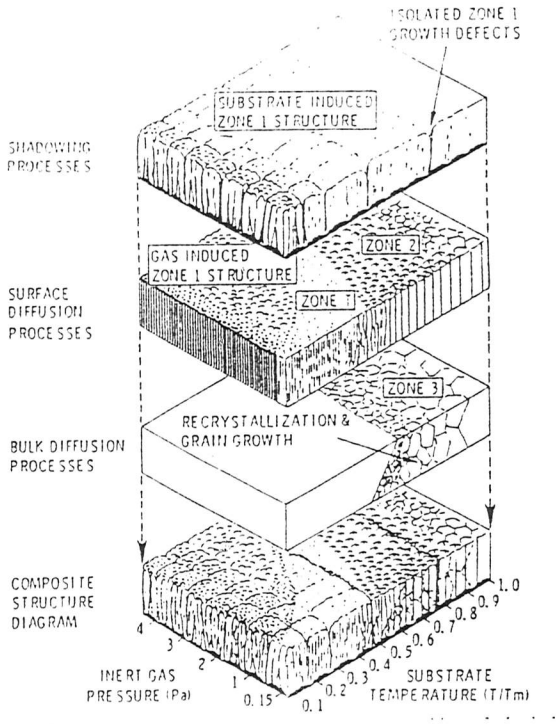

Figure 19. Schematic representation showing the superposition of physical processes which establish structural zones (Ohring 1992).

Zone	T_S / T_M	Structural Characteristics	Film Properties
1 (E)	< 0.3	Tapered crystals, dome tops, voided boundaries.	High dislocation density, hard.
1 (S)	< 0.1 at 0.15 Pa to < 0.5 at 4 Pa	Voided boundaries, fibrous grains. Zone 1 is promoted by substrate roughness and oblique deposition.	Hard.
T (S)	0.1 to 0.4 at 0.15 Pa, ~ 0.4 to 0.5 at 4 Pa	Fibrous grains, dense grain boundary arrays.	High dislocation density, hard, high strength, low ductility.
2 (E)	0.3 to 0.5	Columnar grains, dense grain boundaries.	Hard, low ductility.
2 (S)	0.4 to 0.7		
3 (E)	0.5-1.0	Large equiaxed grains, bright surface.	Low dislocation density, soft recrystallized grains.
3 (S)	0.6-1.0		

Note: (E) refers to evaporated. (S) refers to sputtered.

Table 1. Zone structures in thick evaporated and sputtered coatings (Ohring 1992).

characteristics.

Since the sputtering pressure was kept in the low mTorr range (<0.5 Pa) with substrate temperatures being ~25^{0}C (~0.3 T/T_m, where LiH's T_m is 680^{0}C), the surface morphology is on the edge of zone 1 and zone T. Characteristics of zone 1's oblique deposition and zone T's dense grain boundary arrays can be seen in figure 17 SEM image. Other characteristics from these zones, such as fibrous grain formation, is not seen on the SEM images. Note that the zone model is only a possible conceptual model of the growth kinetics involved.

In addition to the above mechanisms, the rough growth may be associated with mean free path hinderance. The substrates were held ~ 25cm above the target. At the sputtering pressures (~2mTorr), the mean free path of a sputtered atom is ~2.5 cm. A factor of 10 smaller then the distance needed to travel to the substrate. The mean free path is given as

$$\lambda = 1/(2^{0.5}n\sigma) \qquad (10)$$

where n is the number of molecules per volume of the chamber and σ is the cross sectional area of the molecule (Fishbane, et. al. 1993). This large difference in distances should result in numerous collisions of the sputtered atoms with the gaseous environment of the chamber. These collisions would reduce the energy of the atoms arriving at the surface. Since LiH has a low molecular weight relative to the other gases in the chamber (Ar and NH_3), it is early "bumped" out of the way by these heavier atoms and molecules. In our case, lowering the substrate to be

in a closer proximity to the sputtering target could have introduced more problems. These include a large percentage of Ar impingement into the substrate, arcing problems with the plasma, and "splattering" of pure lithium onto the substrate before it could bound with the reactive gas. These "splattering" effects were seen when the LiH was deposited by the triode method mentioned in the TEM section.

As mentioned before in the Band Gap Characterization section, some of the films indicated oxide peaks. The Li_2O formation may have contributed to the rough growth of the films. The difference in densities (LiH is 0.82 g/cm^3 and Li_2O is 2.013 g/cm^3), lattice parameters, and, more importantly, lattice bonding energy differences (stable thermodynamics) could have been contributing factors to promote such growth.

A final possible cause for the rough growth could be the Si substrate. The silicon substrate's different lattice parameter (5.42Å) would prevent heteroepitaxial growth of the LiH crystal. Since the deposited structure is crystalline, polycrystalline formation with no long range order could exist. The roughness of the surfaces could be the indication of polycrystalline growth.

The diffusion characteristics of the lithium on the silicon may have hindered smooth interface growth as well. The kinetics of the system may have allowed the capacity for the lithium to react with the oxide silicon surface in the following manner

$4Li + SiO_2 = 2Li_2O + Si$.

The silicon oxide surface would be present since the silicon

substrate was not deposited in an ultra high vacuum system, nor was it heated to ~800°C to remove any surface oxide contamination. This kinetic reaction could be another explanation for the Li_2O peaks seen in the UV fluorescence characterization.

Since the Si substrate surface could have been a problem in the development of long range smooth planar growth, MgO substrates were used. As mentioned before, MgO has a FCC lattice parameter of 4.20Å. This should allow for heteroepitaxy of the LiH rocksalt structure. Figure 20 is a SEM image of a LiH film deposited on a MgO substrate with NH_3 at 0.85 mTorr. These images clearly show crystallites with multifacets. The surface morphology was rough and favored polycrystalline growth rather then epitaxy. The LiH crystals showed three-dimensional island formation with little lateral growth. This type of nonuniform surface morphology, like the silicon substrate samples, is not suitable for multilayer optics. The roughness of the surface on the MgO could be attributed to similar reasons listed above for silicon. Figure 21 is a larger magnification of this surface.

An attempt to make a LiH/MoN multilayer was done. A multilayer was deposited onto a MgO wafer. It had a theoretical d spacing of 70Å for 40 layer pairs. The reactive gas was NH_3 at 1mTorr. As expected, the film appeared rough (figure 22). A low angle Cu Kα x-ray diffraction method was used to look for a d spacing. X-ray diffraction (XRD) uses incident and reflected x-rays to find the d spacing by focusing the rays at various angles

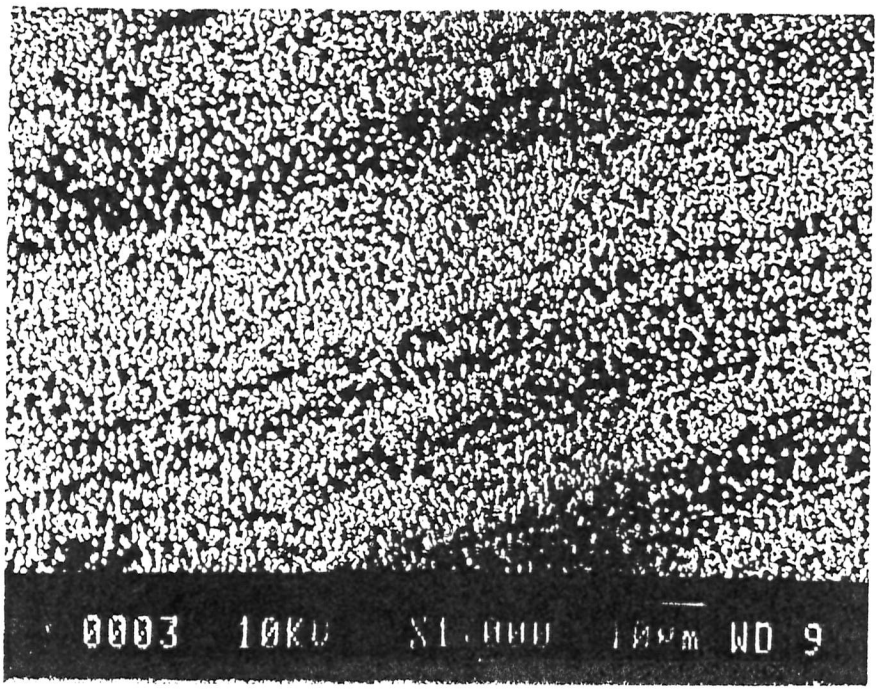

Figure 20. A SEM image of a ~1000Å film of LiH on a MgO substrate. Reactive gas was NH_3 at 0.85 mTorr.

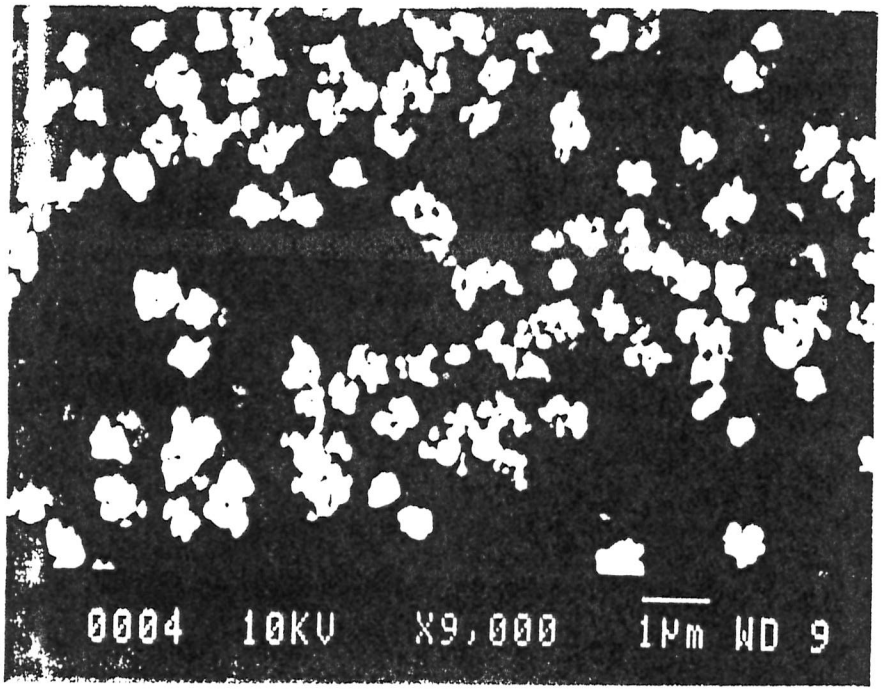

Figure 21. A larger magnification of figure 20. Note the multifacets and island growth of the LiH structure.

on the sample. A peak will occur when the incident angle and d spacing match Bragg's condition (equation 2). XRD scans produced no significant reflected peak. This indicated that no distinct separation between the thin film layers existed. The lack of a peak could be expected since the LiH film showed gaps between crystals in which the MoN could deposit into. To insure that the LiH, not MoN, was the hinderance to the growth of the multilayer stack, a 2000Å MoN film was deposited on Si using NH_3 at 0.85 mTorr. Figure 23 is a SEM image of this film. The image clearly indicates the smooth growth needed to produce distinct interfaces. The film does not indicate any crystallinity. The MoN film was characterized by the Kikuchi method and no electron diffraction patterns were seen. This could indicate amorphous growth or small grain size (recall Kikachi method resolves to ~500Å).

A surprising result occurred when the NH_3 pressure was lowered to ~0.5 mTorr for a similar LiH/MoN multilayer. Figure 24 is a SEM image of this film. This image indicates that the film produced much smoother surfaces. The film's morphology appeared to be in surface tension. This conclusion is deducted by the formation of "cracks" on the surface. This multilayer was placed in the XRD for d spacing characterization. Unfortunately, the sample showed no reflected x-ray peaks, i.e. no evidence of a periodic multilayer.

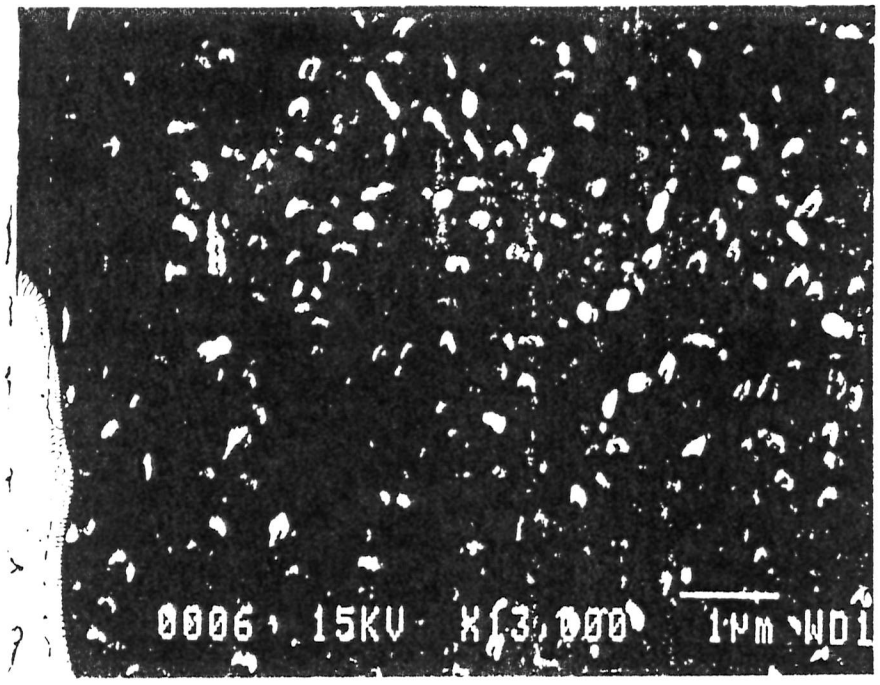

Figure 22. A SEM image of a 3000Å total thickness LiH/MoN multilayer deposited on MgO. Reactive gas was NH_3 at 1 mTorr.

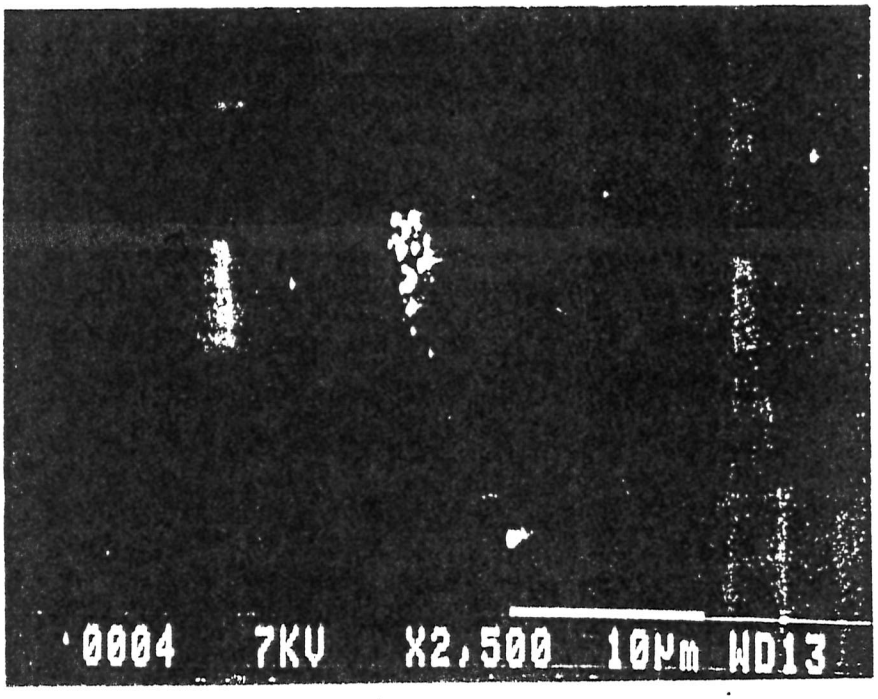

Figure 23. A SEM image of a MoN film on a Si substrate. Note its smooth topology.

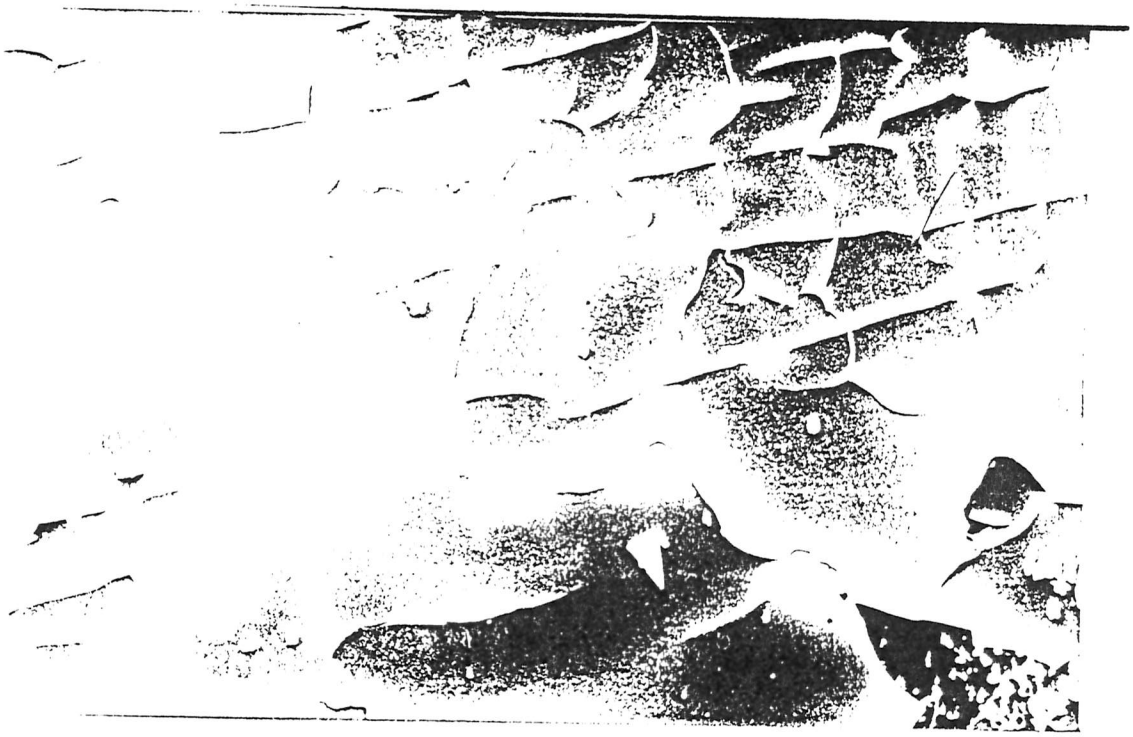

Figure 24. A SEM image of a LiH/MoN multilayer structure. Reactive gas was NH_3 at ~0.5 mTorr. Note the tensile stress the film is in indicated by the surface cracks.

LiF Thin Films

The last type of film investigated was LiF. This thin film has been shown to grow epitaxial. Numerous studies have been done in investigating LiF's electrical and photoemission properties (Saiki, et. al. 1990; Lapiano-Smith 1991). The reactive sputtering gas for this film was semiconductor grade nitrogen triflouride, NF_3. The LiF films were deposited on silicon substrates. The silicon lattice mismatch with LiF would prevent any epitaxial growth. The LiF films deposited in a similar rough manner. Figure 25 is a SEM image of a 500Å film. The surface indicates three-dimensional growth. This type of roughness has been seen in LiF films grown on substrates in which mismatch was significant (Saiki, et. al. 1990). The islands also appeared oblique in shape. This would be typical of zone 1 in the zonal structure model. The rough nature of the films could be a result of the conditions discussed for LiH as well as the problems associated with sputtering this compound. Recall from the Experimental section, the lithium target tended to become an insulator during reactive sputtering using the NF_3 gas. This caused undesirable current and voltage fluctuations, i.e. sporadic sputtering. An attempt to make a LiF/MoN multilayer on Si substrate with 12 layer pairs at a 50Å d spacing was done. The reactive gas, NF_3, would supply each of the appropriate gaseous components, nitride or fluoride, to the sputtered elements. The reactive gas was flowed into the chamber to ~0.5 mTorr. As expected the surface morphology was rough and a XRD

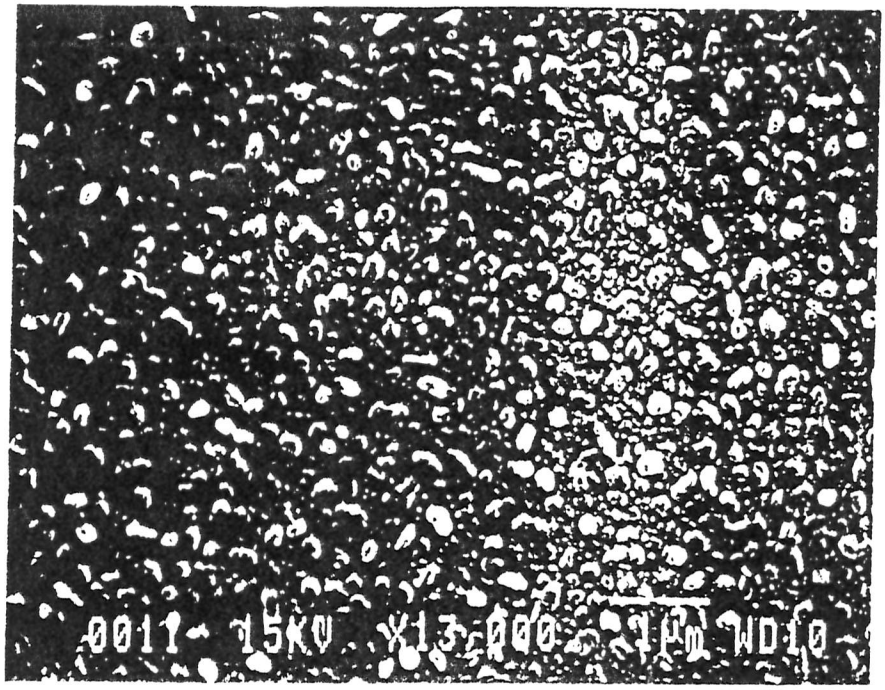

Figure 25. A SEM image of a ~500Å film of LiF on a Si substrate. Reactive gas was NF_3 at 0.4 mTorr

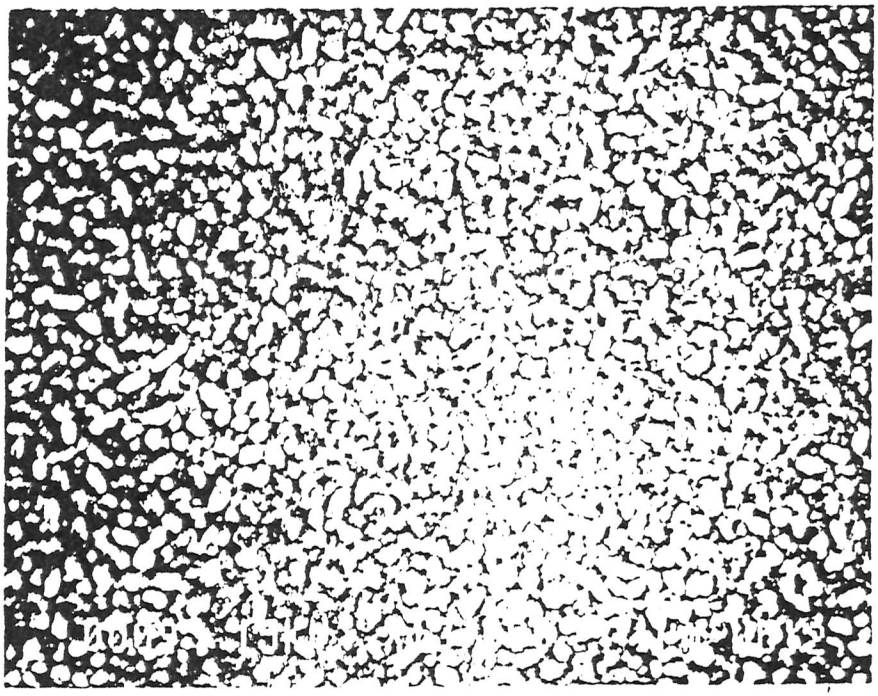

Figure 26. A ~750Å LiF/MoN multilayer structure on a Si substrate. Reactive gas was NF_3 at 0.51 mTorr with added N_2 at 0.49 mTorr (to help insure MoN, not MoF). (X13000 @ 15kV)

scan indicated no periodic multilayer d spacing. Figure 26 is a SEM image of this multilayer.

Conclusion

Are lithium compounds to good to be true? The focus of this research was to investigate the possibility of employing lithium compounds as spacer layers for crystalline based multilayers. Lithium compounds' optical properties in the soft x-ray region make them ideal candidates for such wavelength applications. Reactive gas magnetron sputtering indicated that lithium compound films can be deposited as thin films. Unfortunately, these films indicated extremely rough surface morphology.

The rough growth is believed to be a result of oxide contamination, small mean free path of the sputtered atoms, and/or substrate hinderance. Some of the rough growth matched the morphology described in the zonal model of surface morphology evolution. This type of growth does not allow uniform planar interfaces to exist between thin film pairs. This was indicated by the lack of a reflected x-ray peak in a low angle XRD scans of the multilayers constructed.

The concept of a crystalline optical multilayer was based on the idea that the crystalline epitixial multilayer would and has given rise to such growth behavior. In order to peruse lithium compounds as a spacer layer in multilayer x-ray optics, new methods and deposition techniques which promote smooth growth need to be explored. LiF has been shown, in some cases, to

promote smooth growth by electron beam gun evaporation (Koster, et. al. 1986). Molecular beam epitaxy has also produced smooth alkali halides (Yang and Flynn 1989). In general, techniques which have the ability to control the deposition environment via the reduction of contaminates and the decrease in deposition pressures (an increase in mean free path) will have a greater probability in producing higher quality films.

This research supported that a band gap characterization of lithium compounds seems to be one of the few methods in which these structure can be studied. The transparency of the lithium compound films to electron beams and x-rays made their characterization difficult if not impossible by these techniques.

Acknowledgements

I would like to thank Dr. David D. Allred, my advisor, for his guidance through this project. I would also like to thank Pavel Brovkin for his many hours he spent characterizing my lithium compound films, via SEM and UV floursence. Special thanks to Dr. David Field of TSL TexSEM Laboratories (Provo, Utah) for his Electron Backscatter Diffraction characterization. Thanks to Scott Daniel and Wes Lifferth for technical support. Finally, I would like to thank my wife, Amanda, for her patience with me as I completed this project.

This research was financially supported by MOXTEK, Inc., BYU's Physics and Astronomy Department, and a grant from BYU's Research and Creative Arts Office.

Cited Sources

D. D. Allred, Brigham Young University, Provo, UT, private consultation, (1996).

N. M. Ceglio, J. X-ray Sci. and Tech., **1**, (1989), pp. 7-78.

A. Chambers, R. K. Fitch, and B. S. Halliday, *Basic Vacuum Technology*, Adam Hilger, New York, (1989).

Conference of the Physics of Multilayers, Breckenridge, CO, Sponsored by University of Arizona, (March 1996).

D. Field, TSL TexSEM Laboratories, Private Consultation, (1995).

Fishbane, Gasiorowicz, and Thorton, *Physics for Scientists and Engineers*, Prentice Hall, New Jersey, (1993).

Joy George, *Preparation of Thin Films*, Marcel Dekker, Inc., New York, (1992).

Amit Goswami, *Quantum Mechanics*, Wm. C. Brown Publishers, (1992).

Eric V. Grave, *Discover the Invisible*, Prentice-Hall, Inc., (1984).

A. K. Green, J. Dancy, and E. Bauer, J. of Vac. Sc. and Techn., **7** (1), (1969).

Robert Guenther, *Modern Optics*, John Wiley & Sons, New York, (1990).

F. J. Himpsel, Surface Science, **33**, (1993), pp. 3-14.

N. Hirashita and J. E. Greene, J. Appl. Phys., **70** (9), (1991), pp. 4963-4968.

M. Ikeya and T. Miki, J. Luminescence, **12-13**, (1976), pp. 333-337

K. Kawaguchi and S. Shin, J. Appl. Phys., **67** (2), (1990), pp. 921-929.

D. W. Kim, Y. J. Park, J. G. Lee, and J. S. Chun, Thin Solid Films, **165**, (1988), pp. 149-161.

S. Koster, N. Herres, M. Rey, and K. Reichelt, J. Appl. Phys., **59** (1), (1986), pp. 278-280.

D. A. Lapiano-Smith, E. A. Eklund, and F. J. Himpsel, Appl. Phys. Lett., **59** (17), (1991), pp. 2174-2176.

B. A. Movchan and A. V. Demchishin, Phys. Met. Metallogr., **28**, (1969), pp. 83.

M. Ohring, *The Materials of Science of Thin Films*, Academic Press, Inc. (1992).

M. S. Ortman and E. M. Larsen, J. Am. Ceramic Soc., **66** (9), 1983, pp. 645-648.

H. K. Pew, *The Development of Water Window Soft X-Ray Multilayers for X-Ray Microscopy*, Doctoral dissertation at Brigham Young University, Provo, UT, (1994).

G. I. Pilipenko, D. V. Oparin, and F. F. Gavrilo, Solid State Communications, **57** (11), (1986), pp. 869-871.

A. N. Polienko, M. E. Tabachnik, S. O. Cholakh, A. A. O'Connel-Bronin, Phys. Stat. Sol., **179** (411), (1993), pp. 411-418.

K. Saiki, Y. Nakamura, and A. Koma, Surface Science, **250**, (1991), pp. 27-32.

K. Takayanagi, K. Yagi, and G. Honjo, Thin Solid Films, **48**, (1978), pp. 137-152.

J. Talvacchio and A. I. Braginski, IEEE Transactions on Magnetics, **23** (2), (1987), pp. 859-862.

J. A. Thorton, Ann. Rev. Mater. Sci., **7**, (1977), p. 239.

S. P. Vernon, D. G. Stearns, and R. S. Rosen, Appl. Optics, **32** (34), pp. 6969-6980.

R. C. Weast, editor, *CRC Handbook of Chemistry and Physics*, **58**, CRC Press, Inc., (1977-1978).

M. H. Yang and C. P. Flynn, Phys. Rev. Lett., **62** (21), (1989), pp. 2476-2479.